Enhanced Photoelectrochemical Activity of Sol−Gel Tungsten Trioxide Films through Textural Control

Bin Yang,[†] Yingjie Zhang,[†] Elizabeth Drabarek,[†] Piers R. F. Barnes,[‡] and Vittorio Luca*[,†]

Institute of Materials and Engineering Sciences, Australian Nuclear Science and Technology Organisation, PMB 1, Menai, NSW 2234, Australia, and CSIRO Industrial Physics, P.O. Box 218, Lindfield, NSW 2070, Australia

Received June 16, 2007

Novel mesoporous tungsten trioxide films with enhanced incident photon-to-current conversion efficiencies have been prepared by a sol−gel route from an aqueous precursor solution containing peroxopolytungstic acid (PPTA). For films heated in air at 500 °C, it was found that film texture depended in a precise and reproducible manner on adjustment of the pH of this precursor solution by addition of a small volume of a selected mineral acid. Mesoporous micrometer-thick transparent films were obtained from PPTA without pH adjustment while mesoporous semi-transparent films resulted when the pH was lowered. The transparent films had specific surface areas of 18 m^2/g, average pore diameters of 7.3 nm, and average crystallite sizes of 30 nm. The semi-transparent films possessed specific surface areas of 30 m^2/g, average pore diameters of 12.5 nm, and average crystallite diameters of 17 nm. In the case of the semi-transparent films, electron microscopy indicated that the fundamental crystallites formed part of larger 200−300 nm aggregates which were in turn interconnected to form an open micrometer-length scale porous network. The transparent films did not show this type of porous hierarchy with the absence of micrometer-scale porosity. Photoelectrochemical studies of the films indicated that the hierarchical semi-transparent films exhibited a considerably enhanced photo-response relative to transparent films due to increases in both the interface area and light scattering. After calcination of the semi-transparent films at 500 °C, anodic photocurrents up to an equivalent of 1.4 mA/cm^2 under Air Mass 1.5 equivalent solar irradiation were measured. Our results suggest that film texture is a major factor in determining the performance of the films, and the method reported here provides a simple and convenient means for modulation of this texture.

1. Introduction

Concern over climate change is driving renewed interest in developing clean energy systems, and in this regard, hydrogen has featured prominently as a potential transport fuel of the future.[1] Hydrogen is, however, not readily available and needs to be manufactured. One emissions-free method of hydrogen production, as opposed to steam reforming of hydrocarbons, is via the photoelectrochemical splitting of water using semiconductor electrodes, and there has been an explosion of activity in this field since the first demonstration of the potential of this approach by Fujishima and Honda in 1970.[2]

Tungsten trioxide (WO_3) is an *n*-type semiconductor with a band gap of 2.6 eV and is prominent for its many potential chromogenic applications which are attributable, at least in part, to its favorable electronic properties including the small difference in electrode potential between W(V) and W(IV).[3−6] Tungsten trioxide has also been extensively studied for its gas sensing properties and for the photoelectrocatalytic decomposition of organic molecules.[7] In addition to these applications, tungsten trioxide thin films deposited on a given conducting current collector have yielded among the highest reported efficiencies for the photoelectrochemical splitting of water.[8−13] Ultimately the maximum possible energy conversion efficiency for WO_3 in sunlight (Air Mass 1.5, AM1.5) is limited to about 5% by the material's band gap.[14]

Important considerations in the performance of a semiconductor photoelectrode include the electronic structure of the semiconductor particles making up the film, their size,

* Corresponding author. E-mail address: vlu@ansto.gov.au.
[†] Australian Nuclear Science and Technology Organisation.
[‡] CSIRO Industrial Physics.

(1) Crabtree, G. W.; Dresselhaus, M. S.; Buchanan, M. V. *Phys. Today* **2004**, 39.
(2) Fujishima, A.; Honda, K. *Nature* **1972**, *238*, 37.
(3) Deepa, M.; Sharma, R.; Basu, A.; Agnihotry, S. A. *Electrochim. Acta* **2005**, *50*, 3545.
(4) Cheng, W.; Baudrin, E.; Dunn, B.; Zink, J. I. *J. Mater. Chem.* **2001**, *11*, 92.
(5) Leftheriotis, G.; Papaefthimiou, S.; Yianoulis, P.; Siokou, A.; Kefalas, D. *Appl. Surf. Sci.* **2003**, *218*, 275.
(6) Munro, B.; Kramer, S.; Zapp, P.; Krug, H. *J. Sol-Gel Sci. Technol.* **1998**, *13*, 673.
(7) Solarska, R.; Santato, C.; Jorand-Sartoretti, C.; Ulmann, M.; Augustynski, J. *J. Appl. Electrochem.* **2005**, *35*, 715.
(8) Santato, C.; Odziemkowski, M.; Ulmann, M.; Augustynski, J. *J. Am. Chem. Soc.* **2001**, *123*, 10639.
(9) Miller, E. L.; Marsen, B.; Paluselli, D.; Rocheleau, R. *Electrochem. Solid State Lett.* **2005**, *8*, A247−A249.
(10) Santato, C.; Ulmann, M.; Augustynski, J. *Adv. Mater.* **2001**, *13*, 511.
(11) Santato, C.; Ulmann, M.; Augustynski, J. *J. Phys. Chem. B* **2001**, *105*, 936.
(12) Granqvist, C. G. *Sol. Energy Mater. Sol. Cells* **2000**, *60*, 201.
(13) Baeck, S. H.; Jaramillo, T.; Stucky, G. D.; Mcfarland, E. W. *Nano Lett.* **2002**, *2*, 831.
(14) Murphy, A. B.; Barnes, P. R. F.; Horne, M. B.; Glasscock, J. A.; Grey, I. E.; Plumb, I. C.; Randeniya, L. K. *Int. J. Hydrogen Energy* **2006**, in press.

10.1021/cm071603d CCC: $37.00 Published 2007 by the American Chemical Society
Published on Web 10/24/2007

and how they are connected. While it is well-known that nanoparticulate films can offer an edge in terms of their performance for water splitting applications,[10,15] there appears to be little detailed understanding of the relationship between the precise textural properties and the efficiency of WO_3 photoanodes. In the case of tungsten trioxide it has been clearly demonstrated that there is an optimum crystallinity for the generation of a photocurrent, but it has not been possible to evaluate the effect of texture alone. One reason for this is that there is a relative dearth of available techniques for the precise control of this parameter.

Tungsten trioxide thin films can be synthesized by many different physicochemical means, and there are a numerous examples of interesting nanoscale materials prepared by the use of techniques such as vapor deposition,[16−22] sputtering,[23−25] electrodeposition,[13,26−28] and a variety of sol−gel methods.[4−6]

While the synthesis of WO_3 films by the sol−gel route has several advantages, including low cost, ease with which large surfaces can be coated, control of film thickness, and ability to prepare a range of mesoporous structures, control of the final product microstructure is not straightforward because sol−gel reaction mechanisms are seldom well understood. The aqueous chemistry of the major precursors used to prepare electrochromic tungsten oxide hydrates has been reviewed.[29] For the most part, three main sol−gel routes to tungsten oxide hydrates have been used including acidification of Na_2WO_4 solutions using a cation exchange resin in the proton form,[30] peroxopolytungstic acids (PPTAs) obtained via the direct reaction between tungsten metal and hydrogen peroxide,[31] tungsten alkoxides, and precursor solutions obtained by reaction of $WOCl_4$ with alcohols such as PrOH. Relatively little attention has been paid to the development of methods for the precise control of texture and porosity. Yet texture is important in electrochemical applications where interfacial electron-transfer reactions are concerned. One need only consider the improvement that has been brought about in the performance of silicon based solar cells through micrometer scale control of surface texture[32] and the dye sensitized solar cells[33] which utilize nanoparticulate titania electrode assemblies.

One method to control of texture/porosity on the nanometer length scale is through the surfactant templating approach,[34,35] and this has been exploited to prepare ordered mesoporous thin films of crystalline titania to yield materials with high activity for water splitting.[36] The surfactant templating strategy has also recently been applied to the preparation of poorly crystalline mesotextured tungstate materials, and some have shown interesting chromogenic properties.[26,37−39] However, while such poorly crystalline materials have generally enhanced performance in chromogenic applications, their use for photoelectrochemical water splitting does not immediately follow because this application has the prerequisite of high crystallinity which requires high temperatures. The mesoporous thin films reported so far display limited thermal stability at the temperatures required to remove the template and induce the crystallization necessary to confer high photoactivity. Contamination of the products by residual elements such as S and N present in the surfactants can also have deleterious consequences for the performance of such materials. Thus improved methods for achieving control of texture/porosity need to be developed, and this has formed one of the main objectives of this work.

We describe here a simple method for the preparation of textured WO_3 films with porosity on multiple length scales. The films are prepared by a very simple and reproducible procedure involving the drop casting or doctor blade technique from an aqueous precursor solution of PPTA after careful adjustment of pH by addition of perchloric acid ($HClO_4$). The method of film preparation presented here boasts several advantages including simplicity, low cost, the need for few additives, and precise control of texture. This ability to control texture in a precise manner therefore offers an opportunity for evaluating the influence of texture on photocatalytic performance, and this forms the second major objective of the present work.

2. Experimental Section

Tungsten trioxide films were synthesized by a sol−gel route from an aqueous precursor containing PPTA electrolyte. The precursor was prepared by dissolving 1.8 g of tungsten metal powder (Aldrich Chemical Co., 99.9%) in 60 mL of 30% hydrogen peroxide over about a 6 h period, decomposing the excess hydrogen peroxide by adding a few milligrams of platinum black (Aldrich Chemical Co.),

(15) Wang, H. L.; Lindgren, T.; He, J. J.; Hagfeldt, A.; Lindquist, S. E. *J. Phys. Chem. B* **2000**, *104*, 5686.
(16) Vijayalakshmi, R.; Jayachandran, M.; Trivedi, D. C.; Sanjeeviraja, C. *Synth. React. Inorg., Met.-Org., Nano-Met. Chem.* **2006**, *36*, 89.
(17) Blackman, C. S.; Parkin, I. P. *Chem. Mater.* **2005**, *17*, 1583.
(18) Gesheva, K.; Cziraki, A.; Ivanova, T.; Szekeres, A. *J. Optoelectron. Adv. Mater.* **2005**, *7*, 557.
(19) Gesheva, K.; Szekeres, A.; Ivanova, T. *Sol. Energy Mater. Sol. Cells* **2003**, *76*, 563.
(20) Dimitrova, Z.; Gogova, D. *Mater. Res. Bull.* **2005**, *40*, 333.
(21) Barreca, D.; Bozza, S.; Carta, G.; Rossetto, G.; Tondello, E.; Zanella, P. *Surf. Sci.* **2003**, *532*, 439−443.
(22) Li, Y. B.; Bando, Y.; Golberg, D.; Kurashima, K. *Chem. Phys. Lett.* **2003**, *367*, 214.
(23) Berggren, L.; Niklasson, G. A. *Solid State Ionics* **2003**, *165*, 51.
(24) Cazzanelli, E.; Castriota, M.; Kalendarev, R.; Kuzmin, A.; Purans, J. *Ionics* **2003**, *9*, 95.
(25) Akl, A. A.; Kamal, H.; Abdel-Hady, K. *Phys. B: Condens. Matter.* **2003**, *325*, 65.
(26) Baeck, S.-H.; Choi, K.-S.; Jaramillo, T. F.; Stucky, G. D.; McFarland, E. W. *Adv. Mater.* **2003**, *15*, 1269.
(27) Meulenkamp, E. A. *J. Electrochem. Soc.* **1997**, *144*, 1664.
(28) Yang, B.; Li, H.; Blackford, M.; Luca, V. *Curr. Appl. Phys.* **2006**, in press.
(29) Livage, J.; Guzman, G. *Solid State Ionics* **1996**, *84*, 205.
(30) Chemseddine, A.; Morineau, R.; Livage, J. *Solid State Ionics* **1983**, *9−10*, 357.
(31) Kudo, T.; Okamoto, H.; Matsumoto, K.; Sasaki, Y. *Inorg. Chim. Acta* **1986**, *111*, L27−L28.
(32) Lakhtakia, A.; Ashok, S. *Sol. Energy Mater. Solar Cells* **1997**, *46*, 137.
(33) O'Regan, B.; Grätzel, M. *Nature* **1991**, *353*, 737.
(34) Alberius, P. C. A.; Frindell, K. L.; Hayward, R. C.; Kramer, E. J.; Stucky, G. D.; Chmelka, B. F. *Chem. Mater.* **2002**, *14*, 3284.
(35) Grosso, D.; Soler-Illia, G. J.; Crepaldi, E. L.; Cagnol, F.; Sinturel, C.; Bourgeois, A.; Brunet-Bruneau, A.; Amenitsch, H.; Albouy, P. A.; Sanchez, C. *Chem. Mater.* **2003**, *15*, 4562.
(36) Tang, J.; Wu, Y.; McFarland, E. W.; Stucky, G. D. *Chem. Commun.* **2004**, 1670.
(37) Hillhouse, H. W.; Van, Egmond, J. W.; Tsapatsis, M. *Langmuir* **1999**, *15*, 4544.
(38) Pan, J. H.; Lee, W. I. *Chem. Mater.* **2006**, *18*, 847.
(39) Chen, D.; Li, Z.; Yu, C.; Shi, Y.; Zhang, Z.; Tu, B.; Zhao, D. *Chem. Mater.* **2005**, *17*, 3228.

and finally diluting the solution to 100 mM by adding about 50 mL of 2-propanol to improve the stability. After removal of the platinum black by filtration, the resulting precursor solution had a pH of 1.58. The pH of the precursor solution could be systematically lowered from 1.58 to 0.2 by adding a few drops of 1 M perchloric acid ($HClO_4$). Lowering the pH of the precursor altered the appearance of the resulting films in a progressive manner from transparent to semi-transparent. The thin films were deposited by doctor blade or drop-casting the precursor onto conducting indium doped tin oxide (ITO) coated glass at room temperature and then dried at 60 °C. Finally, the films were calcined in air at 500 °C for 30 min to form a crystalline WO_3 layer. After calcination, the films adhered strongly to the ITO glass. Thick and homogeneous films were made by repeated deposition−calcination cycles. Control of film thickness was achieved through either control of solution concentration or through repetition of the deposition annealing cycles.

Scanning electron microscopy (SEM) images were recorded using a JEOL JSM6400 electron microscope. X-ray diffraction was performed using a Panalytical X'Pert Pro diffractometer with an X'cellerator multichannel detector employing real time multiple strip technology. Ni-filtered Cu Kα radiation ($\lambda = 0.154$ nm) was used. Light absorption was calculated from diffuse reflectance spectra that were measured at ambient temperature using a Cary 500 spectrophotometer equipped with a Labsphere Biconical Accessory. To avoid interference in the thin WO_3 layer, we scratched the WO_3 powder from the film and mixed it homogeneously with MgO in a ratio of 1:4. Diffuse optical transmission measurements were also made on the films themselves using the same equipment.

Photocatalytic activity of the films was investigated using a standard three electrode cell with a flat quartz window to allow illumination of the electrodes. Solar light was simulated using an Oriel 6271 ozone-free xenon lamp, with an Oriel 61945 water filter fitted. The spectrum of the lamp was calibrated precisely by the Australian National Measurement Institute because solar simulators are often not well characterized in the UV range.[14] The irradiance of the xenon lamp incident on the WO_3 films was 86 mW/cm^2 measured using an Oriel Instruments miniature thermopile detector (model 71751). The integrated intensity of the xenon lamp spectrum used here (normalized to an AM1.5 intensity of 100 mW cm^{-2}) has ~1.3 times the intensity of sunlight for photon energies greater than the band gap of WO_3 (2.6 eV). Multiplying measured photocurrents by a factor of $100/(86 \times 1.28) = 0.91$ yields AM1.5 equivalent values.[14]

The efficiency is determined according to

$$\eta = j_p(1.23 - V_{bias})/E_S$$

where j_p is the photocurrent (mA/cm^2), E_S is the incident radiation energy (mW/cm^2), V_{bias} is the cell bias between the working and counter electrodes, and 1.23 eV is the Gibbs free energy per electron for the water splitting reaction. For photoelectrodes fabricated with an embedded photovoltaic or arranged in a tandem configuration, V_{bias} is often assumed to be zero for the purposes of calculating efficiency.[14]

Incident photon-to-current conversion efficiencies (IPCEs) were obtained using the following relation:

$$\text{IPCE}\ (\lambda) = 100 \times 1241 \times j(\lambda)/\lambda I_0(\lambda)$$

where λ is the wavelength of light in units of nm, $j(\lambda)$ is the photocurrent density in mA cm^{-2} under illumination at λ, and $I_0(\lambda)$ is the incident-light intensity in mW cm^{-2} at j.

In this work we focus on a detailed study of two types of films as typical examples: transparent films prepared at pH = 1.58 and semi-transparent films prepared at pH = 0.8.

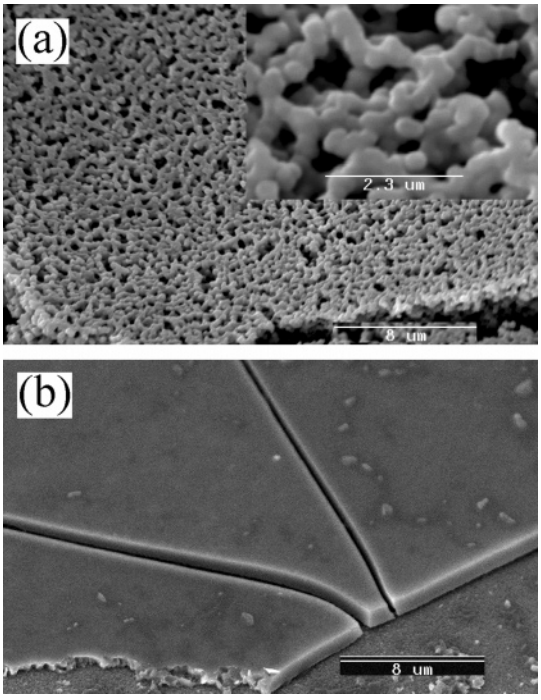

Figure 1. SEM images of (a) the semi-transparent film prepared at pH = 0.8 and (b) the transparent film prepared at pH = 1.58 after calcination at 500 °C. Inset is a higher magnification image of the film in part a and shows that the mesoporous film is composed of interconnected WO_3 particles with diameters of about 300 nm while the transparent film has a relatively smooth surface at the length scale of observation.

3. Results

3.1. Characterization of Films. SEM images of the semi-transparent and transparent films prepared from solutions at pH of 0.8 and 1.58 after calcination at 500 °C are shown in Figure 1. These SEM images were recorded with the film surface tilted at about 40° with respect to the incident electron beam to image both the surface and the cross section of the WO_3 layer and to yield its thickness. The images show that the semi-transparent WO_3 film consists of an open three-dimensional (3D) network of interconnected droplet-like nanoparticles with diameters in the range of 100−300 nm. This mesoporous structure forms through the colloidal condensation of the molecular precursor species during the evaporation of solvent at 60 °C. The nature of this condensation process is at present not well understood and is beyond the scope of the present study. The inset to Figure 1a is a high magnification image of the semi-transparent film and shows that these films are quite uniform over some tens of micrometers with the presence of a few microcracks. We have observed that the structure and texture is preserved up to a calcination temperature of 550 °C. This temperature is close to the limit of stability of the ITO-coated glass substrate.

In comparison with the semi-transparent films, the SEM image of transparent films (Figure 1b) prepared without the addition of perchloric acid (pH = 1.58) indicated smooth surfaces with occasional cracks. Although the structure at this length scale appears smooth, this does not preclude the existence of porosity on smaller length scales. It proved difficult to create transparent films thicker than 1.5 μm

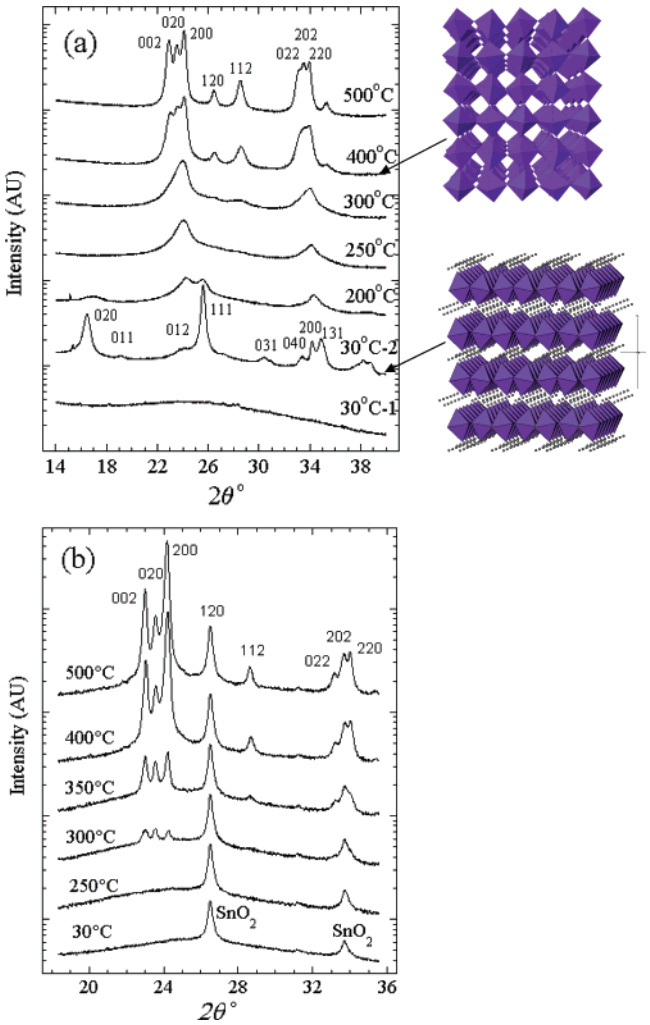

Figure 2. Stack plot of the in situ X-ray diffraction patterns of (a) semi-transparent and (b) transparent film on a glass substrate, after heating to increasing temperatures. Structures are those of monoclinic WO_3 and tungsten oxide hydrate $WO_3 \cdot H_2O$.

because of poor adhesion of the WO_3 layer to the ITO glass during annealing.

The structural evolution of the transparent and semi-transparent WO_3 films as a function of temperature was studied by in situ X-ray powder diffraction in the range 30−500 °C (Figure 2). The XRD patterns of the as-deposited semi-transparent film (Figure 2a) indicate that the tungstate layer was amorphous at room temperature (30 °C-1) as no sharp reflections were observed. The pattern of the as-deposited film contained only a very broad hump centered at $2\theta = 25°$. However, this film was unstable and extremely hygroscopic, rapidly absorbing water from the atmosphere (at ambient temperature of 25 °C and relative humidity of 60%). In fact, small water droplets could be observed to develop within minutes. After 24 h in ambient air, the amorphous film transformed to yellowish tungsten oxide hydrate (H_2O_4W or $WO_3 \cdot H_2O$) as was evidenced by the presence several reflections (30 °C-2). In particular, the tungstate phase obtained under these conditions has an orthorhombic unit cell ($a = 0.52477$ nm, $b = 1.07851$ nm, $c = 0.51440$ nm, and space group of *Pmnb*).[40,41] No such transformation was observed at room temperature for the transparent film.

At 200 °C, the tungsten oxide hydrate in the semi-transparent film showed the existence of WO_3 nanocrystals, indicated by the presence of two very broad peaks at 24 and 34.5° 2θ. However, the correlation length/crystallite size of the WO_3 crystals at this temperature was very small, about 7 nm, when evaluated using the Scherrer equation, $D = 0.9\lambda/(\beta \cos \theta)$, where λ is X-ray wavelength and β represents the full width at half-maximum (FWHM) of the peak at 2θ, in this case at 24°. At 250 °C, the transformation to WO_3 was complete, because the reflections of the tungsten oxide hydrate disappeared. The nanocrystals grew in size at 400 °C, as indicated by the appearance of the three characteristic reflections of monoclinic ($P2_1/n$) WO_3 at $2\theta = 23.0$, 23.6, and 24.1°. The crystallization was complete at about 500 °C, because the intensities of these three peaks centered at 23.6° 2θ increased to their maximum values at this temperature even though they continued to sharpen. The relative intensities of these three reflections were close to that observed in a random WO_3 powder pattern indicating that this semi-transparent film exhibited only a weak degree of preferred orientation. In addition, the average size (or crystallite diameter) of the crystallites comprising the semi-transparent film increased to 17 nm ($\beta = 0.45°$ for the (112) peak at $2\theta = 28.5°$) for this sample. It was observed that the final morphological structure of semi-transparent WO_3 films at 500 °C was independent of the initial state of the film. In other words, heating either the amorphous or the tungsten oxide hydrate film resulted in the same mesoporous structure at higher calcination temperatures.

The XRD pattern of the transparent film (Figure 2b) displayed a significant degree of preferred orientation as could be deduced from the relative intensities of the triplet of reflections centered at 23.6° 2θ. Even though these transparent films were obviously more crystalline at a given temperature compared with the semi-transparent films, the photocurrents that could be obtained from them were always significantly lower. The average domain size calculated after heating to 500 °C was 30 nm, almost twice that of the semi-transparent film. This result suggests that another synthetic parameter is the dominant factor influencing film performance, namely, film texture.

The porosity of the films was evaluated by scraping the films from the slides and measuring the nitrogen adsorption−desorption isotherms. Figure 3 shows the isotherms and the average pore size distribution for the semi-transparent and transparent films. Both samples gave isotherms which were of Type IV, clearly highlighting the fact that the films have significant mesoporosity. The BET surface area of the semi-transparent film was found to be approximately twice that of the transparent film (32 versus 18 m^2/g), and the average mesopore diameters were 12.5 and 7.3 nm, respectively. This factor of 2 difference in porosity is entirely consistent with the difference in crystallite size. For perfect isolated 17 (semi-transparent) and 30 nm (transparent) spherical particles the calculated specific surface areas would be 49 and 27 m^2/g, respectively. These values are only about 50% larger than

(40) Szymanski, J.; Roberts, A. *Can. Mineral.* **1984**, *22*, 685.
(41) Gerand, B.; Nowogrocki, G.; Figlarz, M. *J. Solid State Chem.* **1981**, *38*, 312.

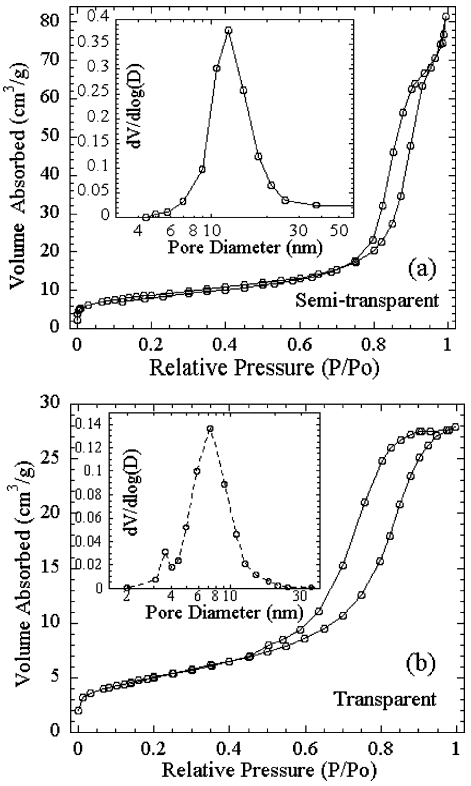

Figure 3. Adsorption−desorption isotherms and average pore size distribution for the (a) semi-transparent and (b) transparent films calcined at 500 °C.

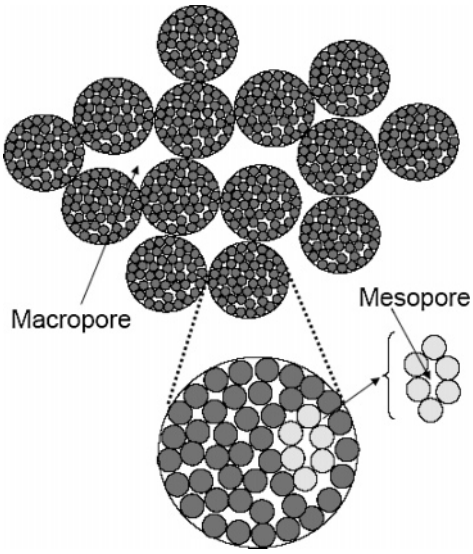

Figure 4. Model of the hierarchical semi-transparent WO_3 films.

the measured values. Loss of surface area due to particle−particle contacts is probably responsible for this discrepancy.

The model of the semi-transparent film that is suggested by the data presented here so far is shown in Figure 4. In this model for the semi-transparent film the fundamental 17 nm WO_3 crystallites measured by XRD are clustered into aggregates that are about 200−300 nm in diameter that can be easily observed in the SEM images. The individual crystallites within the aggregates define the mesoporosity of the system. The 200−300 nm nanometer scale aggregates observed by SEM in turn define a network of micrometer-sized pores by partial sintering, and we term this the secondary structure.

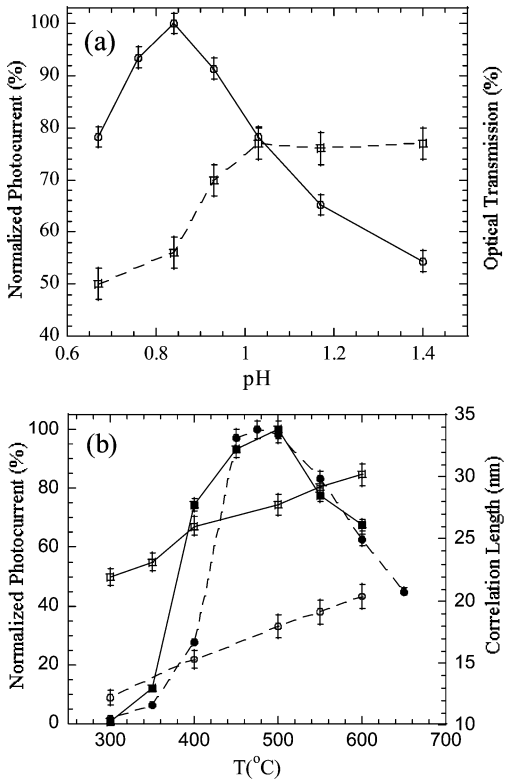

Figure 5. (a) Photocurrent dependence (○) and the corresponding visible (white) light diffuse transmittance (□) as a function of the pH of PPTA solution used for film formation (500 °C). (b) Photocurrent of transparent (■) and semi-transparent (●) films and the crystal correlation length of the transparent film (□) and semi-transparent (○) films as a function of calcination temperature.

3.2. Photochemical Properties. Figure 5a shows the dependence of photocurrent on the pH of the precursor solution after adjustment with 1 M perchloric acid for films with a similar mass per unit area after these films had been calcined at 500 °C. This bell-shaped curve shows a clear photocurrent maximum for films prepared from PPTA solutions whose pH was adjusted to 0.8. Films calcined at 500 °C also had different visual appearances depending on the final pH of the precursor solution used for their preparation. The as-prepared PPTA solution had a pH of 1.58 and when used for film preparation gave rise to smooth transparent films. In contrast, films prepared from the precursor PPTA solution whose pH was lowered to around 0.8 by the addition of mineral acid and corresponding to the peak in photocurrent had a semi-transparent opaque appearance. The terminology "semi-transparent" and "transparent" will be used for films prepared at these two pH values which are the focus of the remainder of this paper. To discount the possibility that films prepared at calcination temperatures of 500 °C underwent interaction with the ITO substrate we removed a tungsten trioxide film calcined at 500 °C from the original ITO substrate, reapplied a new film, and re-measured the photocurrent. The fact that identical results were obtained suggests absence of interaction up to at least this temperature.

Shown in Figure 5a is the variation in optical transmission (of broadband light) for the films fired at 500 °C that were prepared from precursor solutions at the different pH values. It is clear that as the films changed from being visually

transparent to semi-transparent with decreasing pH, the optical transmission was reduced. The major reduction in optical transmission occurred at a pH value at which the photocurrent was maximized. This suggests that the light harvesting efficiency of the films increased as the pH was reduced, and this was presumably related to the texture of the film. However, it is clear from the photocurrent curve in Figure 5a that optical absorption is not the only factor influencing photoactivity, because photocurrent declined at pH < 0.8. Because, as will be shown in due course, the band gap of the transparent and semi-transparent films are the same in increased light absorption, the difference is not due to different band gap absorption.

The dependence of photocurrent on calcination temperature for a typical semi-transparent film prepared at pH = 0.8 is shown in Figure 5b. A clear maximum was observed at a heating temperature of between 475 and 500 °C. A similarly shaped curve, also with a maximum at around 500 °C, was observed for transparent films prepared from PPTA precursor solution to which no perchloric acid had been added. The present results therefore confirm that there is a strong dependence of photocurrent on calcination temperature for films prepared from PPTA at a given pH. Because crystallite size (measured using XRD as discussed below) varied linearly with calcination temperature as shown in Figure 5b it is clear that the bell-shaped dependence of photocurrent on calcination temperature is not determined entirely by the crystallite size. It follows, for the case of the semi-transparent film, that a calcination temperature of at least 300 °C corresponding to a crystalline size of at least 12 nm was required for the observation of photocurrent. The lack of a defined correlation between crystallite size and photocurrent is further emphasized by the fact that the transparent film, which had a significantly larger domain/crystallite size of 22 nm after heating to 300 °C, continued not to show any significant photocurrent until this temperature. In fact this value of crystallite dimension for the transparent film calcined at 300 °C already exceeded the value obtained for the semi-transparent film at 500 °C.

The electrochemical and photocatalytic properties of semi-transparent and transparent films were investigated by comparing semi-transparent and transparent films with the same weight of WO_3 per unit area (0.5 mg/cm^2). The semi-transparent film exhibited a stronger electrochemical response than the transparent film. Figure 6a shows the cyclic voltammograms (CVs) for hydrogen intercalation−deintercalation in the calcined WO_3 films in 0.1 M sulfuric acid. During the CV, the color of the film changed reversibly on reduction from pale yellow to dark blue and reverted back to pale yellow on oxidation. This electrochromic process corresponds to the reversible change between WO_3 and the blue tungsten bronze (H_xWO_3), as a result of the insertion and extraction of hydrogen. Figure 6a illustrates clearly that the semi-transparent film generates a higher photocurrent for both oxidation and reduction of the transparent films. Because the current increased quasi-linearly, the geometrical contact resistance, R_c, between the semi-transparent film and the electrolyte can be gauged from the slope of anodic and cathodic scans of the films in the electrolyte. Two points

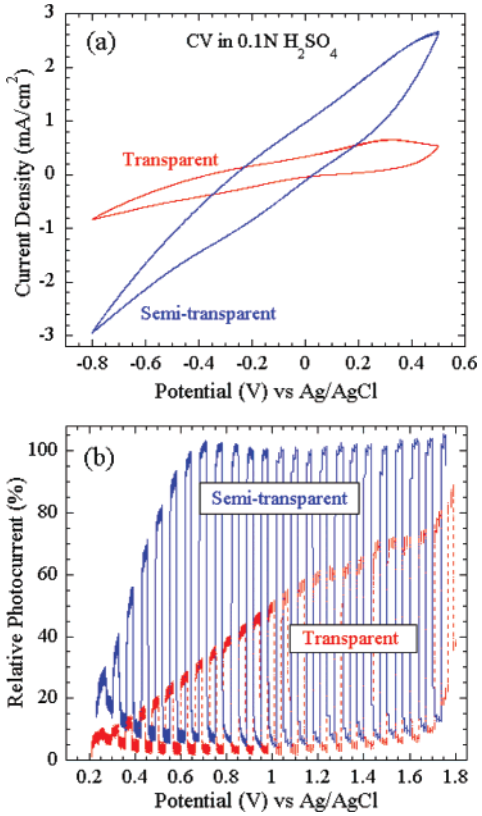

Figure 6. (a) CVs (−0.8 to 0.2 V vs Ag/AgCl, 20 mV/min ramp) of annealed (at 500 °C for 30 min) transparent and semi-transparent WO_3 films in 0.1 N H_2SO_4 aqueous solution. The cathodic and anodic peak currents correspond to the formation and oxidation of the hydrogen tungsten bronze (H_xWO_3) during cycling. (b) Potentiodynamic scans (30 mV/s) under chopped illumination from a tungsten lamp for the semi-transparent and transparent films.

(0.5 V, 2.7 mA/cm^2 and −0.8 V, −3.0 mA/cm^2) were chosen from the CV of semi-transparent film to calculate the resistance by applying the equation $R_c = (0.5 + 0.8)/(2.7 + 3) = 228\ \Omega\ \text{cm}^2$.

For the transparent film, $R_c = (0.5 + 0.8)/(0.51 + 0.79) = 1000\ \Omega\ \text{cm}^2$. The R_c of the semi-transparent film was about a quarter that of the transparent film. The difference in specific surface areas (mesoporosity) discussed above only accounted for half of this difference in R_c. This suggests that the efficiency of charge transport, both within the electrolyte and the electrode, is important, and the difference in secondary structure between the two films might account for the remaining difference in R_c. The micrometer scale pores in the semi-transparent film (Figure 2a) may well assist transport of both charge and evolved gas through the electrolyte phase, relative to the denser structure of the transparent film (Figure 2b).

Figure 6b shows potentiodynamic scans (30 mV/s) under chopped illumination for the two films, in 1 M H_2SO_4 and 0.1 M CH_3OH. The photochemical reaction of CH_3OH in the electrolyte has been studied by Santato et al.[11] The photocurrent is the difference between the light current and the dark current. From Figure 6b it is evident that there were two major differences between the two scans: (1) the saturation photocurrent of the semi-transparent film (100%) was about 40% higher than that of the transparent film (60%); and (2) for the semi-transparent film, the photocurrent rose

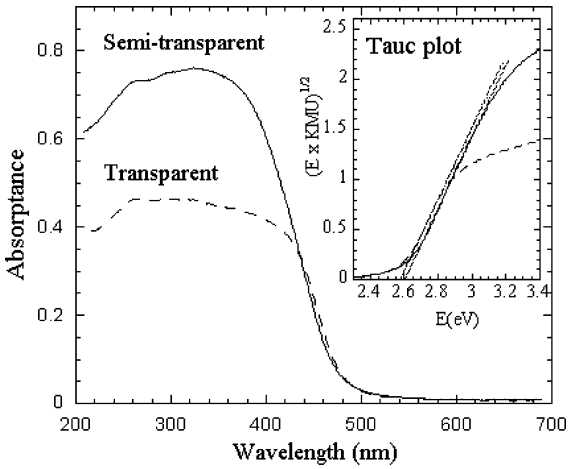

Figure 7. Light absorption of the WO_3 powders obtained from semi-transparent and transparent films calcined at 500 °C as a function of wavelength, at room temperature. The data were collected using a diffuse reflectance spectrometer. The inset shows a Tauc plot for an indirect band gap semiconductor calculated from the data.

rapidly with increasing potential. In particular, for the semi-transparent film, the photocurrent increased more or less linearly up to the saturation current (100%) as the potential rises from 0.2 to 0.6 V and then reached a plateau at higher voltages. For the transparent film the photocurrent increased linearly up to 60% while the potential rose from 0.2 to 1.2 V, and then the light current and dark current increased equally so that the photocurrent remained at the saturated value. It is interesting to note that there was a fourfold difference in slope (photocurrent vs potential) between the two films which matched the corresponding slope difference in the CV measurements. On the basis of this observation, we can conclude that the photocurrent rises quasi-linearly as the potential increases from the "onset potential" to the "saturation potential", and its slope corresponds to a contact resistance between the working electrode material and the electrolyte. In the case of the semi-transparent sample, the resistance was lower, so the photocurrent consequently saturates at lower bias. In fact, the slope is strongly related to the texture of the film. This phenomenon was also observed in the photocurrent measurements when the electrolyte contained only 1 M H_2SO_4 and no CH_3OH.

The texture of the semi-transparent films had a strong influence on the energy conversion efficiency of the films for splitting water to hydrogen and oxygen in sunlight. Because higher photocurrents could be reached at a lower bias potential with the semi-transparent film, this would lead to improvements in conversion efficiency compared to the transparent films. It seems therefore at this stage that these textural properties may be more important than the degree of crystallographic preferred orientation in defining the water splitting efficiency as has been previously suggested by Santato et al.[11]

In Figure 7 are shown UV−vis absorption spectra of the transparent and semi-transparent films calculated from the diffuse reflectance data. For both samples, the absorption onset occurred near 460 nm. The band gap of all the films was 2.6 eV corresponding to an indirect band gap of purely crystalline WO_3. These values were determined using a Tauc plot which shows the square root of the Kubelka−Munk function (KMU = $(1 - R)^2/2R$, where R is the reflectance) multiplied by photon energy as a function of photon energy (Figure 7, inset).[15,42] The absence of any significant "red" or "blue" shift suggests that the average domain size in each of the films was well above the quantum confinement limit for WO_3 in accordance with the XRD results. It was also evident that the film texture does not influence the band gap. However, a notable difference between the two spectra was that the integrated intensity of the absorption peak of the semi-transparent film was about 30% larger than that of transparent film. This was confirmed by diffuse reflectance and transmission measurements of glass coated with the same mass per unit area of transparent or semi-transparent WO_3 which indicated a similar ratio of total absorption as that seen in Figure 7. The more effective absorption of light by the semi-transparent material probably results from an increased path length of short wavelength light in the film due to scattering from the 3D network (see Figure 2a). This is favorable for the conversion of incident light to photocurrent.

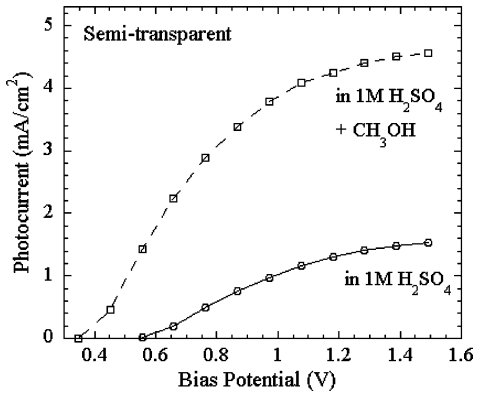

Figure 8. Dependence of photocurrent on bias potential (the difference between the working and counter electrodes) of the semi-transparent films in 1 M H_2SO_4 with and without adding 0.2 mol/L of CH_3OH, respectively. The WO_3 layer thickness is about 2.4 nm, and illumination from the water filtered xenon lamp is 86 mW/cm^2.

To determine which film synthesis conditions achieved the highest photoactivity, we synthesized mesoporous semi-transparent films of various thicknesses by using sequential deposition and measured the photocurrent as a function of layer thickness. The optimum thickness of the semi-transparent film was found to be about 2.8 μm, and this thickness was used for all subsequent experiments. Figure 8 shows the photocurrent of the best film as a function of applied bias in 1 M H_2SO_4 before and after addition of 0.1 mol/L of methanol. The addition of methanol resulted in an unexpected threefold increase in saturation photocurrent from 1.5 to 4.5 mA/cm^2 (1.4 to 4.1 mA/cm^2 equivalent photocurrent under AM1.5) and a negative shift of the current onset potential by about 0.2 V. The photocurrent is comparable with that reported by Santato et al.;[8] however, they observed only a twofold increase in photocurrent with the addition of methanol which can be explained by the well-known current doubling effect.[43] The photocurrent action spectrum (IPCE) for the semi-transparent WO_3 film at 1 V versus the SCE (Figure 9) showed peak efficiency of about 40% at a

(42) Butler, M. A. *J. Appl. Phys.* **1977**, *84*, 1914.
(43) Morrison, S. R.; Freund, T. T. *J. Chem. Phys.* **1967**, *47*, 1543.

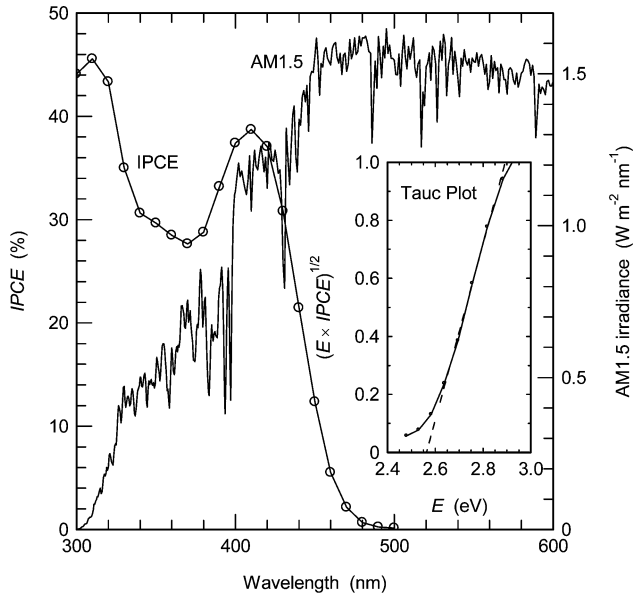

Figure 9. Photocurrent action spectrum (incident photon-to-current conversion efficiency, IPCE) of semi-transparent WO_3 electrode in 1.0 M H_2SO_4 at 1 V vs SCE. The irradiance of the AM1.5 spectrum is also shown for comparison. Inset: Tauc plot for the indirect semiconductor derived from the IPCE measurements.

wavelength of 410 nm. Also shown for comparison is the irradiance of the AM1.5 spectrum. By convolving the IPCE curve with the photon flux, $I(\lambda)$, derived from the AM1.5 spectrum, an estimate of the AM1.5 photocurrent can be calculated:[14]

$$j_{\text{calculated}} = e\int_0^{\infty} \text{IPCE}(\lambda)\, I(\lambda)\, \mathrm{d}\lambda$$

where e is the electronic charge. In this case the calculated photocurrent using the IPCE(λ) in Figure 9 was $j_{\text{calculated}} = 1.15$ mA/cm^2, and the measured photocurrent under 86 mW/cm^2 illumination from a xenon lamp was 1.2 mA/cm^2 at 1 V versus SCE. Using the approximation described in the experimental section this measured current is equivalent to $j_p = 1.1$ mA/cm^2, similar to $j_{\text{calculated}}$. The inset in Figure 9 shows a Tauc plot derived from the IPCE measurement. The band gap derived was equivalent to that derived from the diffuse reflectance measurements shown in Figure 7.

4. Discussion

As stated in the introduction to this study, to be able to produce high efficiency films in the context of water splitting, one must first be able to identify the most important factors for the generation of high activity. Santato et al.[8] came to the conclusion that crystallite size and degree of preferred orientation were the dominant factors influencing photoactivity and relegated porosity to a secondary factor. However, the texture of a semiconductor electrode is potentially important as it can have a number of beneficial consequences such as an increase in the number of semiconductor−electrolyte interfaces at which electron-transfer reactions take place and therefore transport of charged species as well as improving light harvesting efficiency.

Papaefthimiou et al.[44] have demonstrated the benefits of texturing on the hundreds of micrometer scale on the electrochromic response of WO_3 electrodes made using electron gun deposition. The use of texturing on the micrometer scale is also a common method for improving the efficiency of silicon photovoltaics.[32] It was the advent of particulate TiO_2 thin films with mesoporous texture using the sol−gel approach that helped to make solar cells based on dye-sensitization a promising and intensively studied technology.[33]

In the present work we have sought to achieve controlled texturing using an extremely simple synthetic method. We have demonstrated that films formed by lowering the pH of PPTA solutions using a mineral acid can result in vastly different textures relative to films formed from PPTA solution whose pH was not adjusted. Our data unequivocally show that the semi-transparent films produced at a pH of 0.8 have twice the surface area and larger average mesopore diameters (12.5 compared with 7.3) relative to transparent films produced from PPTA solutions whose pH was not adjusted. Moreover, the variation induced by pH adjustment appears to be systematic in the sense that it generates a bell shaped variation in photo-response as one moves from high (transparent films) to low (semi-transparent films) pH. While both extremes of pH yield mesoporous films, the SEM images clearly show that the semi-transparent films also have a porosity on the micrometer length scale that is not observed in the transparent films. This porosity on multiple length scales is preserved and may even be promoted, by heating to 500 °C because sintering of aggregates probably occurs at these temperatures. This temperature also appears to produce the optimum crystallinity for water splitting. However, it is not yet clear whether reduction in photocurrent after calcination at temperatures beyond 500 °C results from the collapse of mesoporosity due to further crystal growth and sintering or is possibly linked to alteration of the ITO substrate.

The hierarchical semi-transparent films produced here (Figure 4) are much more active than the transparent films, and this is likely due to an increase in solid−electrolyte interface area and/or related to the light absorbed within the film. While it is difficult to disentangle these two effects, they are both ultimately related to the texture of the films. In comparison with the tungsten trioxide materials investigated here, mesoporous TiO_2 derived from block copolymers does not show this hierarchical structure because the only mesoporosity is created through packing of the 5−10 nm fundamental crystallites.[36]

So far, few techniques are available for the controlled generation of mesoporous texture in WO_3 films which should result in similar performance improvements in water splitting. One exception is the study by Baeck et al.[26] where sodium dodecyl sulfate was used as a texturing agent to produce lamellar tungsten oxides. In the study by Baeck et al., 800 nm thick lamellar WO_3 films displayed 26% increased photocurrent relative to a reference film prepared without a mesotexturing agent. That study concluded that the improvement in photocurrent yield was attributed to the texture of the films, which agrees with what we have observed. It is

(44) Papaefthimiou, S.; Leftheriotis, G.; Yianoulis, P. *Solid State Ionics* **2001**, *139*, 135.

well-known from the earlier study of Santato et al.[8] and confirmed here now that crystallite dimensions can be quite different for films produced in different ways and that this profoundly influences the photocurrent that can be expected. Santato et al. claimed that the dominant factor affecting photoactivity was WO_3 crystallite orientation, and no measure of this was provided by the Baeck study either. In the present study we have attempted to quantify all of these related factors for films produced using novel, simple, and easily reproducible methods. From inspection of the triplet reflections centered at around 23.5° 2θ in the XRD patterns it is apparent that our semi-transparent mesoporous films have orientations approximating that of bulk WO_3 while the transparent mesoporous films have crystallite orientations approximating that of Santato et al. That the former are far more active than the latter suggests that orientation is subordinate to texture in determining activity. In other words the overriding factor appears to be the nature of the porosity, and the improved performance of our semi-transparent films is probably mostly due to the enhancement in ion transport and electron transfer occurring at the electrode−electrolyte interface in these hierarchical films. The trapping or scattering of light within such a structure may ultimately be the reason for the activity, but this in turn comes down to a textural effect.

In another relevant and recent study,[9] photocurrents of about 3 mA/cm^2 for optimized films (2.8 μm thickness) prepared using low-temperature reactive sputtering were obtained. In this case, 0.33 M H_3PO_4 solution was used as the electrolyte. While the thickness of the films investigated in the Miller study is similar to that in ours their measurements were made in electrolyte solutions containing no hole scavengers. They referred to their films as compact; however, they provided no information on porosity or microscopy of their materials, and thus it is hard to gauge the importance of texture for their film performance. The XRD patterns that were reported are similar to those of our semi-transparent films.

Our results help clarify the connection between film texture and photocurrent capacity and emphasize the need to produce an open connected network of semiconductor nanoparticles as an important element in obtaining high performance.

While we have succeeded in preparing micrometer thick hierarchical WO_3 films by a simple pH adjustment of the precursor PPTA solution, the exact changes in solution chemistry on pH adjustment leading to a particular texture on calcination remain to be illuminated, and this will be the subject of ongoing studies. However, some comments are in order. It is known that when tungsten metal is dissolved in peroxide solution the primary solution species appears to be diperoxo tungstate dimers.[45] Kudo et al.[46] have ventured that the yellow glassy solid product produced on evaporation of such solutions is related to one of the main polytungstate cations. Clearly, condensation of these diperoxo species can occur on evaporation. In the present work amorphous materials are also produced initially on evaporation of PPTA solutions at pH of 1.58 and 0.8. Herein we have observed crystalline tungsten oxide hydrate formed on evaporation only of the PPTA solution adjusted to low pH. This hydrate then transforms to a hierarchical interconnected structure on calcination. The PPTA solution whose pH was not lowered using acid gave glassy solids that never crystallized at room temperature and on calcination did not produce hierarchical porosity. This points to the fact that different polycations form on evaporation of PPTA solutions of different pH which restructure in different ways on calcination.

5. Conclusions

We have demonstrated here for the first time that the pH used for the preparation of PPTA solutions can strongly influence the texture of WO_3 films formed from these solutions offering a simple and precise method for control of texture. The following additional conclusions can be drawn from our experimental results:

(1) Semi-transparent films produced by pH adjustment to a value of 0.8 gave saturation photocurrents under AM1.5 equivalent sunlight and 1 M H_2SO_4 of 4.1 mA/cm^2 and 1.4 mA/cm^2, with and without 0.1 M CH_3OH, respectively.

(2) The contact resistance of the semi-transparent film was about four times lower than that of the transparent film, and this appears to be linked to the difference in film texture.

(3) The results clearly show that higher porosity allows a higher saturated photocurrent at lower bias potential.

While the band gap of the two film types (transparent and semi-transparent) are about the same, the semi-transparent film absorbed more UV light than the transparent film probably as a result of light scattering within the film. This together with an enhancement in the number of solid−solution interfaces are the properties of these films that contribute to their higher performance.

Acknowledgment. The authors gratefully acknowledge the assistance of Dr. Ian Plumb of CSIRO and Ms. Julie Glasscock of the University of New South Wales for assistance with photochemical measurements.

CM071603D

(45) Dickman, M. H.; Pope, M. T. *Chem. Rev.* **1994**, *94*, 569.
(46) Kudo, T.; Oi, J.; Kishimoto, A.; Hiratani, M. *Mater. Res. Bull.* **1991**, *26*, 779.